Development of a shock circle model based on the two-dimensional distribution to assess the performance of a supersonic ejector used in refregeration systems

K. Megdouli

Development of a shock circle model based on the two-dimensional distribution to assess the performance of a supersonic ejector used in refregeration systems

K. Megdouli
Institut Jean Le Rond D'Alembert, Sorbonne Université, Faculté des Sciences et Ingénierie, Campus Pierre et Marie Curie 75252 Paris Cedex 05, France
Email: karima.magdouli@sorbonne-universite.fr

***Abstract*—** This article presents a thermodynamic model that offers the advantage of simplifying the calculation process and effectively explaining the complex mechanism of double throttling within the ejector for real gases. The paper begins by describing the model's assumptions and the calculation procedure. It then assesses the influence of the various parameters on yields. The validity of the model is confirmed by validation using several data sets. In addition, the ejector model is applied to the simulation of an ejector refrigeration cycle in order to guarantee its reliability and its ability to predict the performance of thermodynamic cycles.

Keywords—Ejector; Velocity distribution; Shock circle

I. INTRODUCTION

In Europe, 40% of the electric energy consumption is due to heating and cooling systems. So, increasing their efficiency is a fateful step to reduce heat losses and carbon dioxide emission [1]. The majority of heat pump systems operate with Hydrofluorocarbons (HFCs), such as R134a with Global Warming Potential (GWP) of 1430. To act against global warming and reduce greenhouse gas emissions, the European regulation prohibits the use of certain HFCs according to their GPW. From 2030, the refrigerant authorized on refrigeration installations must have a GWP less than 150. As a result of the legislation, R1234yf is introduced as an environmentally friendly fluid [1]. To address the increasing demand for cooling, numerous novel thermodynamic cycles have been devised and analyzed to harness low-level heat sources, including industrial waste heat or solar heat. Among these refrigeration cycles designed for low-grade heat utilization, such as absorption cycles [2], adsorption cycles [3], and ejection cycles [4], ejection cycles have garnered a growing interest.

Depending on the specific application, ejector sizes can vary significantly, ranging from several meters for desalinating seawater to just a few centimeters for vehicle air-conditioning systems. In the context of refrigeration, employing ejectors offers several advantages. Firstly, it can minimize the energy losses associated with traditional expansion valves in conventional refrigeration cycles. Secondly, in Ejector Refrigeration Systems (ERS), compression can be achieved using low-grade thermal sources like solar energy or industrial waste heat, thereby reducing reliance on fossil fuels and curbing greenhouse gas emissions.

Furthermore, ejectors have the benefit of having no moving parts, making them straightforward to construct, install, and maintain at a low cost.

An ejector consists of two nozzles, known as the primary and secondary nozzles, which are designed to converge and then diverge, as depicted in Fig. 1. These two nozzles are aligned, with the primary nozzle situated within the secondary nozzle. The fundamental principle of a supersonic ejector can be summarized as follows [2]: Initially, the high-pressure primary flow (designated as P_p and T_p) undergoes expansion as it passes through the primary nozzle, ultimately reaching supersonic speeds at the nozzle's exit. This supersonic flow effectively captures and draws in the secondary flow, which operates at a lower stagnation pressure (P_s). Subsequently, these two flows, characterized by different velocities and temperatures, mix within the mixing duct, resulting in the exchange of both momentum and energy. Finally, the mixed flow undergoes compression within the diffuser section. This entire process serves two primary purposes: firstly, the entrainment of the secondary flow, and secondly, its compression. Consequently, the performance of an ejector is typically evaluated using two distinctive parameters [3]:

- The compression Ratio (r): The compression ratio, denoted as r, represents the relationship between the total pressure at the ejector outlet (P_b) and the pressure at the secondary inlet (P_s). It quantifies the ratio of these two pressure values.
- The entrainment Ratio (U): The entrainment ratio, symbolized as U, signifies the ratio between the mass flow rate of the secondary flow ($\dot{m}_2$) and that of the primary flow ($\dot{m}_1$). It measures how much the secondary flow is drawn in relative to the primary flow.

979-8-3503-4284-0/23/$31.00©2023 European Union

2023 14th International Renewable Energy Congress (IREC) | 979-8-3503-4284-0/23/$31.00 ©2023 IEEE | DOI: 10.1109/IREC59750.2023.10389272

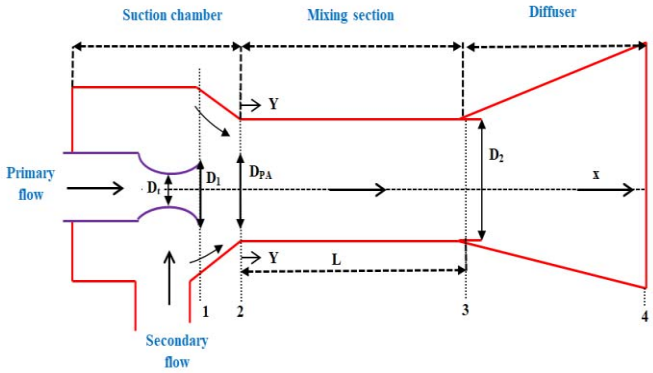

Fig. 1. Schematic diagram of the ejector

Fig. 2 displays a graph illustrating the behavior of an ejector, specifically showing the entrainment ratio in relation to the back pressure. This curve reveals three distinct operational zones when maintaining constant inlet pressures (Both primary and secondary flow) and gradually increasing the back pressure.

- In the on-design region, both the primary and secondary flows are choked, meaning that changes in the back pressure do not impact the entrainment ratio. Importantly, information about the outlet conditions does not affect the upstream choked section.
- Beyond a critical point, as the back pressure rises, the entrainment ratio declines because the secondary flow is no longer choked. The ejector operates in the off-design region, and its efficiency decreases as a result.
- If the back pressure is further increased past a breakdown pressure, a reverse flow occurs at the secondary inlet, causing the ejector to malfunction. Typically, the choking condition of the secondary flow is identified when the sonic line reaches the ejector wall. At this point, the secondary flow becomes entirely supersonic.

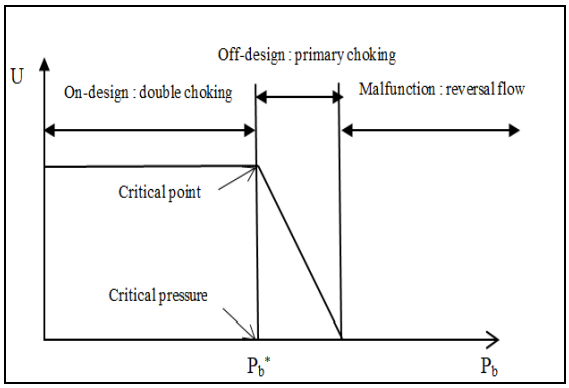

Fig. 2. A graph depicting the performance curve of an ejector

II. Real gas implementation

The selection of the Peng-Robinson Equation of State (PREOS) was motivated by its extensive application within the chemical industry [5, 6]. Equation (1) is utilized to determine the pressure (P) using coefficients derived from Equation (2) for a and Equation (3) for b. Additionally, the parameters a and b for a pure substance are computed based on the critical pressure (P_c), critical temperature (T_c), and acentric factor (ω).

$$P = \frac{RT}{v-b} + \frac{a}{v(v+b)+b(v-b)} \quad (1)$$

Mixed flow

$$a = \frac{0.45724 R^2 T_c^2 k}{P_c} \quad (2)$$

$$b = \frac{0.0778 R T_c}{P_c} \quad (3)$$

$$k = (1 + (0.37464 + 1.54226w - 0.26992w^2)(1 - T_r^{0.5}))^2 \quad (4)$$

III. MODELING AND ANALYSIS

The 2-D flow dynamics equations governing the behavior of an ejector (Fig. 1) are inherently intricate, encompassing principles of mass conservation, momentum conservation, and energy conservation. To facilitate the analysis, certain simplifying assumptions are applied without sacrificing the comprehensiveness of the study.

1- The primary flow inside the ejector is evenly distributed in the radial (r) direction.

3- The pressure and temperature of the secondary flow exhibit uniform distribution along the radial (r) direction.

4- The ratio of the length (L_x) to the diameter (D_2) is approximately 1.50, ensuring that the primary flow can expand and fully accelerate the secondary flow within the suction chamber. This causes the secondary flow to reach the choking condition at the cross-section designated as A–A.

5- The pressure of the secondary flow within the suction chamber maintains a uniform distribution and remains equal to its inlet pressure.

The mass flow rate of the primary flow through the nozzle (m_p) when it reaches the choking condition can be determined as indicated below [7]:

$$m_p = P_p A_t \left(\frac{\gamma \psi_p}{R_g T_p}\right)^{\frac{1}{2}} \left(\frac{2}{1+\gamma}\right)^{\frac{\gamma+1}{2(\gamma-1)}} \quad (5)$$

Where, ψ_p represents the coefficient that accounts for the isentropic efficiency of compressible flow within the nozzle. P_p and T_p denote the static pressure and temperature of the primary flow at the nozzle's inlet, respectively.

By applying principles of mass conservation, energy conservation, and utilizing isentropic flow equations, we establish the connection between the nozzle's exit diameter (D_1), Mach number at the nozzle exit (M_1), nozzle throat diameter (D_t), and Mach number at the nozzle throat (M_t) as follows [7]:

$$\frac{D_1}{D_t} = \left[\frac{2+(\gamma-1)M_1^2}{2+(\gamma-1)}\right]^{\frac{\gamma+1}{4(\gamma-1)}} \left(\frac{1}{M_1}\right)^{\frac{1}{2}} \quad (6)$$

$$\frac{T_p}{T_t} = 1 + \frac{1}{2}(\gamma-1)M_1^2 \quad (7)$$

$$V_1 = M_1 \sqrt{\gamma R_g T_1} \quad (8)$$

Considering the temperature (T_1) and velocity (V_1) of the primary flow at the nozzle exit, and taking into account that the primary flow expands completely within the suction chamber (as per assumption 4), we can represent the

ambient pressure of the expanding flow as equivalent to the pressure of the surrounding secondary flow (denoted as P_s). By applying principles of energy conservation and utilizing isentropic flow equations in gas dynamics, we derive the following equations [7]:

$$\frac{P_p}{P_s}=\left[1+\frac{1}{2}(\gamma-1)M_{PA}^2\right]^{\frac{\gamma}{r-1}} \quad (9)$$

$$\frac{T_p}{T_{PA}}=1+\frac{1}{2}(\gamma-1)M_{PA}^2 \quad (10)$$

$$V_{PA}=M_{PA}\sqrt{\gamma R_g T_{PA}} \quad (11)$$

$$\frac{D'_{PA}}{D_1}=\left[\frac{2+(\gamma-1)M_{PA}^2}{2+(\gamma-1)M_1^2}\right]^{\frac{\gamma+1}{4(\gamma-1)}}\left(\frac{M_1}{M_{PA}}\right)^{\frac{1}{2}} \quad (12)$$

Where: the practical effective expanded diameter is linked to the isentropic efficiency (ψ_{exp}) within the suction chamber. This relationship is typically expressed as follows, considering the parameters: P_1 (primary flow pressure at nozzle exit), M_{PA} (Mach number), T_{PA} (temperature), V_{PA} (velocity in the x direction) of the primary flow at section A–A, and D'_{PA} (effective expanded diameter of the primary flow in an ideal process):

$$D_{PA}=D'_{PA}/\sqrt{\psi_{exp}} \quad (13)$$

Considering that the isentropic coefficient for the primary flow is represented as ψ_p and for the secondary flow as ψ_s, it's logical to account for the combined impact of friction losses from both the primary and secondary flows within the suction chamber by utilizing a product of ψ_p and ψ_s. In other words, this product factorizes the collective effect on friction losses attributed to both flow :

$$\psi_{exp}=\psi_p\times\psi_s \quad (14)$$

The velocity in the radial (r) direction at section A–A closely resembles an exponential distribution, we can employ the following equation to describe the variation of this variable relationship [7]:

$$\frac{v_r}{V_{PA}}=\left(1-\frac{r}{R_2}\right)^{\frac{1}{n}} \quad (15)$$

Where v_r is velocity at radius r in the x direction, V_{pA} is velocity of the primary flow in the x direction at section A–A. When we apply the natural logarithm to both sides of the previous equation, we obtain the following result:

$$n=\frac{\ln(1-r/R_2)}{\ln(1-v_r/V_{PA})} \quad (16)$$

To determine the value of n, we should utilize the conditions present at the shock circle. The velocity of sound at the shock circle is [5]:

$$v_r=\sqrt{\gamma R T_{sA}} \quad (17)$$

n is finally written in the following form [5] :

$$n=\frac{\ln(1-D_{PA}/D_2)}{\ln(\sqrt{T_{sA}/T_{PA}}/M_{PA})} \quad (18)$$

Define the mean flow velocity and the mass flow rate of the secondary flow at section A–A as follows [5]:

$$\bar{V}_{sA}=\frac{\int_{R_{PA}}^{R_2}2\pi r v_r dr}{\pi(R_2^2-R_{PA}^2)} \quad (19)$$

$$m_s=\int_{R_{PA}}^{R_2}\rho_r v_r dr \quad (20)$$

Using assumption (3) and the preceding equations, we finally obtain [7]:

$$\bar{V}_{sA}=\frac{2V_{PA}}{R_2^2-R_{PA}^2}\left[\frac{nR_2^2}{n+1}\left(1-\frac{R_{PA}}{R_2}\right)^{\frac{n+1}{n}}-\frac{nR_2^2}{2n+2}\left(1-\frac{R_{PA}}{R_2}\right)^{\frac{2n+1}{n}}\right] \quad (21)$$

$$m_s=\frac{2\pi P_s V_{PA}}{R_g T_{sA}}\left[\frac{nR_2^2}{n+1}\left(1-\frac{R_{PA}}{R_2}\right)^{\frac{n+1}{n}}-\frac{nR_2^2}{2n+2}\left(1-\frac{R_{PA}}{R_2}\right)^{\frac{2n+1}{n}}\right] \quad (22)$$

Ultimately, in the case of an ideal gas, the energy balance relationship can be articulated as follows [8]:

$$m_p c_p T_p+m_s c_s T_s=m_p\left(c_p T_{pA}+\frac{1}{2}V_{pA}^2\right)+m_s\left(c_p T_{sA}+\frac{1}{2}\bar{V}_{sA}^2\right)+E_{loss} \quad (23)$$

$$E_{loss}=\frac{1}{2}(1-\psi_p)m_p V_1^2+\frac{1}{2}(1-\psi_{exp})m_p V_{PA}^2+\frac{1}{2}(1-\psi_s)m_s V_{sA}^2 \quad (24)$$

IV. RESULTS AND DISCUSSION

A. Validation of the ejector model

The experimental data from Huang et al. [7] was employed to validate the proposed ejector model, and Table 1 demonstrates a strong concurrence between the two sets of data. By referring to Table 1, we can affirm that the presented model exhibits superior accuracy in its predictions of the ejector's entrainment performance.

B. Response Surface Methodology (RSM)

RSM employs a sensible design approach and employs several quadratic regression equations to establish a functional connection between factors and response values. The theoretical examination of crucial structural parameters, especially the intricate effects of multi-parameter interactions on the performance of the ejector within the BER cycle, can be quite complex. Analyzing how each parameter affects the ejector's performance allows us to discern the trend of their respective influences on the ejector's performance.

TABLE 1: THE OUTCOMES OF OUR CURRENT STUDY ARE JUXTAPOSED WITH THE RESULTS DERIVED FROM THE EXPERIMENTAL DATA PRESENTED BY HUANG ET AL.[9]

P_p(MPa);T_p(°C)	P_s(MPa);T_s(°C)	$U = \dot{m}_s/\dot{m}_p$		
		Huang et al. [9]	Present work	Error (%)
0.604;95	0.04;8	0.1859	0.1839	1.07
0.538;90	0.04;8	0.2246	0.2278	1.42
0.465;84	0.04;8	0.2880	0.2792	3.05
0.4;78	0.04;8	0.3257	0.3302	1.38
0.604;95	0.0473;12	0.2350	0.2503	6.51
0.538;90	0.0473;12	0.2946	0.2971	0.84
0.465;84	0.0473;12	0.3398	0.3602	6

In this study, the nozzle throat diameter D_t ranged from 1.86 mm to 3.64 mm, while the exit nozzle diameter D_1 varied between 3.5 mm and 6.5 mm. The boundary conditions for the ejector remained constant throughout our simulations, including a primary flow inlet temperature of 90°C, a primary flow inlet pressure of 5.38 bar, a secondary flow inlet pressure of 0.434 bar, a secondary flow inlet temperature of 10°C, and an ejector outlet pressure of 1.12 bar.

The quadratic representation of this correlation can be found in eqn. 25:

$$y = \beta_0 + \sum_{i=1}^{n} \beta_i x_i + \sum_{i=1}^{n} \beta_{ii} x_i^2 + \sum \sum_{i<j} \beta_{ij} x_i x_j + \varepsilon \qquad (25)$$

In this equation, y represents the output variable (U), β signifies the coefficient, x stands for the input variable (namely, D_t and D_1), and ε denotes the error in observations. Fig. 2 shows the changes in the RSM for ejector performance at various D_t, and D_1. We found that the ejector's performance is notably responsive to variations in D_t, as evidenced by the steepness of its contour line.

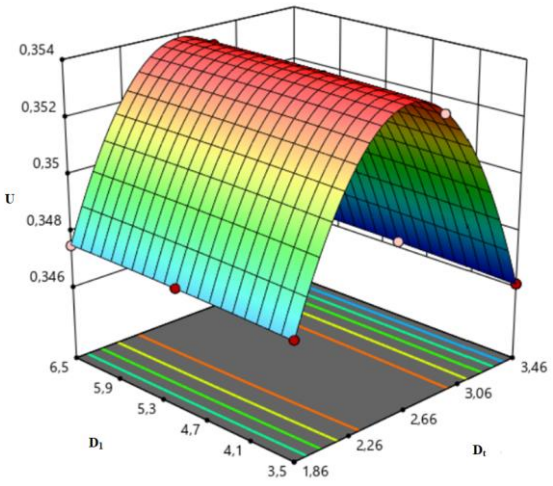

Fig. 3. Response surface analyses of the entrainment ratio with D_t and D_1

However, it was found that there exists an optimal value for D_t, which led to the optimization of the ejector. To delve deeper into the impact of this parameter on the ejector's performance, individual variable analyses is conducted. During the single-variable analysis, it is necessary to maintain the other variable constant, D_1= 4.5 mm. The RSM analysis of the data indicates a strong quadratic relationship with a favorable regression coefficient between the independent factor variables and U. The quadratic polynomial equation for U, which incorporates the independent variables, can be formulated as follows:

$$U = 0.3538 - 0.0006D_t + 0.0001D_1 - 0.0069D_t^2 \qquad (25)$$

Fig. 4 depicts how the ejector's performance changes with varying values of D_t (nozzle throat diameter). Initially, as D_t increases, the ejector performance improves, but after reaching a certain point, it starts to decline significantly. Subsequently, U experiences a rapid increase as D_t continues to rise. The maximum U value of 0.353 is achieved when D_t is set at 2.66 mm, and afterward, it begins to decrease with further increases in D_t. This illustrates that within the range of nozzle throat diameter variations, there is a substantial U variation of approximately 116%, highlighting the significant influence of D_t on the ejector's performance.

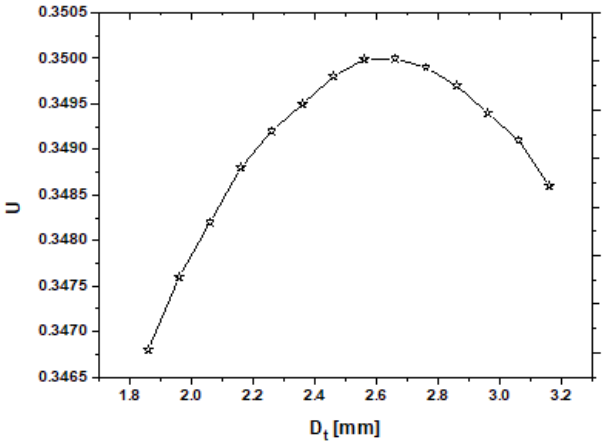

Fig. 4. Variation in U with D_t

C. Sensitivity analysis

After validating the ejector model, it is implemented in an ERS driven by low-grade heat sources to enhance its performance, Fig. 5. This integration enables the refrigeration system to operate more sustainably and economically, making it a viable and efficient solution for cooling applications powered by low-grade heat [10]. The successful application of the ejector model contributes to the overall advancement and innovation of environmentally friendly and energy-efficient refrigeration technologies.

The coefficient of performance (COP) of the ERS studied is given by the following expression:

$$COP = \frac{\dot{Q}_{evaporator}}{\dot{Q}_{generator} + \dot{W}_{pump}} \qquad (26)$$

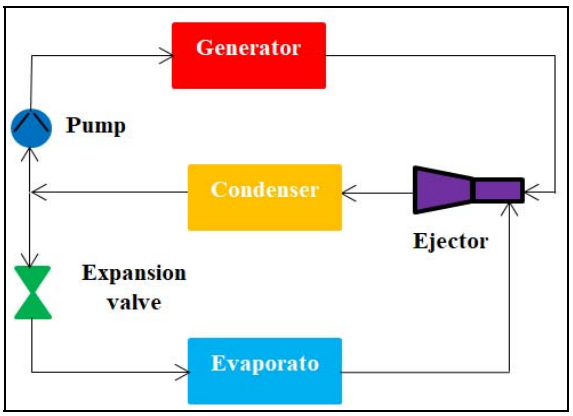

Fig. 5. Schematic of an ejector refrigeration system (ERS)

Fig. 6 illustrates the impact of the evaporator temperature

on the COP, considering a condenser temperature of 35 °C and three different values of the generator temperature. It is observed that for evaporation temperatures exceeding 10°C, elevating the generator temperature will lead to a decrease in COP.

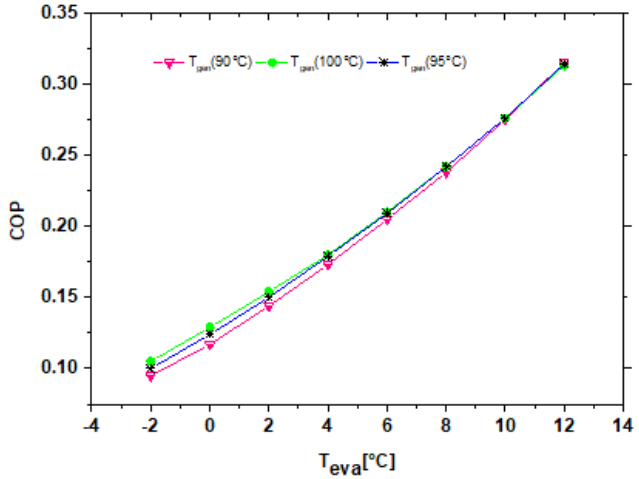

Fig. 6. Variation in the COP with the evaporator temperature for different generator temperatures at T_{cond} = 35 °C

V. CONCLUSIONS

The impact of geometry on ejector performance has been assessed in order to optimize the design of the ejector. Through the application of Response Surface Methodology for investigating the impact of two parameters (D_t and D_1) on ejector performance, we determined that optimizing the value of the diameter of the nozzle throat could enhance ejector performance. The sensitivity analysis demonstrated that the sensitivities of ejector performance to these parameters followed a descending order: D_t>D_1.

Consequently, when aiming to optimize ejector performance, D_t should take precedence. These results provide clarity regarding the hierarchy and influence of multiple variables in the analyses. Following the validation of the ejector model, it is integrated into a refrigeration system powered by low-grade heat sources to improve its operational efficiency. The influence of design parameters on the thermodynamic performance of the system studied is investigated. It is observed that when the system operates with a generator temperature of 90°C, an evaporation temperature of 12 and a condensation temperature equal to 35°C, the system has an efficiency of 0.31. We can confirm that the ejector refrigeration system demonstrates a high level of competitiveness and efficiency.

ACKNOWLEDGMENTS

The author thanks the Institut Jean Le Rond D'Alembert at Sorbonne Université for its support with the dissemination of this research work.

REFERENCES

[1] S. Braccio, N. Guillou, N. Le Pierres, N. Tauveron, H.T. Phan (2023). Mass-flowrate-maximization thermodynamic model and simulation of supersonic real-gas ejectors used in refrigeration systems. Thermal Science and Engineering Progress, 2023, vol 37, pp. 101615.

[2] S. Braccio, H. Trieu Phan, M. Wirtz, N. Tauveron, N. Le Pierrès (2022). Simulation of an ammonia-water absorption cycle using exchanger effectiveness, Appl. Therm. Eng., vol 213, pp. 118712. 3

[3] A. Godefroy, M. Perier-Muzet, N. Mazet (2019). Thermodynamic analyses on hybrid sorption cycles for low-grade heat storage and cogeneration of power and refrigeration. Appl. Energy 2019, vol 255, pp. 113751.

[4] S. Elbel, N. Lawrence. Review of recent developments in advanced ejector technology, Int. J. Refrig, 2016, vol 62, pp. 1–18.

[5] J.S. Lopez-Echeverry, S. Reif-Acherman, E. Araujo-Lopez. Peng-Robinson equation of state: 40 years through cubics. Fluid Phase Equilib., 2017, vol 447, pp. 39–71,

[6] Julián C. Restrepo, Andrés F. Bolaños-Acosta, José R. Simões-Moreira. Short nozzles design for real gas supersonic flow using the method of Characteristics. Applied Thermal Engineering 2022, vol. 207 pp. 118063.

[7] G. Besagni, R. Mereu, F. Inzoli. Ejector refrigeration: A comprehensive review, Renew. Sustain. Energy Rev. 2016, vol 53, pp. 373–407.

[8] Z. Aidoun, K. Ameur, M. Falsafioon, M. Badache. Current Advances in Ejector Modeling, Experimentation and Applications for Refrigeration and Heat Pumps. Part 1: Single-Phase Ejectors, Inventions. 2019, pp. 4: 15.

[9] B.J. Huang, J.M. Chang, C.P. Wang, V.A. Petrenko. A 1-D analysis of ejector performance. International Journal of Refrigeration 1999, vol 22, pp. 354–364.

[10] K. Megdouli, T. Gholizadeh , B. Tashtoush , P. Cinnella , A. Skorek-Osikowska. Optimization of carbon dioxide ejector expansion transcritical refrigeration system with ANOVA and NSGA-II. International Journal of Refrigeration 2023, vol 158, pp. 173-189.